Supplement to: Ice thickness in the Columbia River Basin, Canada

Ben M. Pelto,[1*] Fabien Maussion,[2] Brian Menounos,[1] Valentina Radić,[3] Maurice Zeuner[1,4],

[1]*Natural Resources and Environmental Studies Institute and Geography Program, University of Northern British Columbia, Prince George, Canada*

[2]*Department of Atmospheric and Cryospheric Sciences, Universität Innsbruck, Innsbruck, Austria*

[3]*Department of Earth, Ocean and Atmospheric Sciences, University of British Columbia, Vancouver, Canada*

[4]*Faculty of Physics and Earth Sciences, Leipzig University, Leipzig, Germany*

Correspondence: Ben M. Pelto <pelto@unbc.ca>

ICE THICKNESS MAPS

This section contains detailed maps (Figures S1– S7) of ice thickness observations with shaded topographic relief from LiDAR DEMs and surface slope. The LiDAR DEMs used are from Pelto and others 2019.

GLACIER OUTLINES

To represent our glaciers within OGGM, we extract glacier outlines from the Randolph Glacier Inventory (RGI) V6.0 (Pfeffer and others, 2014) which date to 2005 in the Basin. Nordic and Illecillewaet glaciers are improperly represented in RGI so we corrected their outlines (Figure S8).

Nordic Glacier has three branches: The east and central branches of the glacier meet and form a common terminus, but their intersection is overlain with a thick medial moraine (Figure S9), which is not mapped in the RGI. The western branch of Nordic Glacier has had a separate terminus since before the earliest regional inventory (1985) but was designated part of Nordic Glacier (Bolch and others, 2010). Separating the western branch of Nordic Glacier, and connecting its eastern branch (Figure S8) reduced model bias.

*Present address: Geography Program, University of Northern British Columbia, Prince George, Canada.

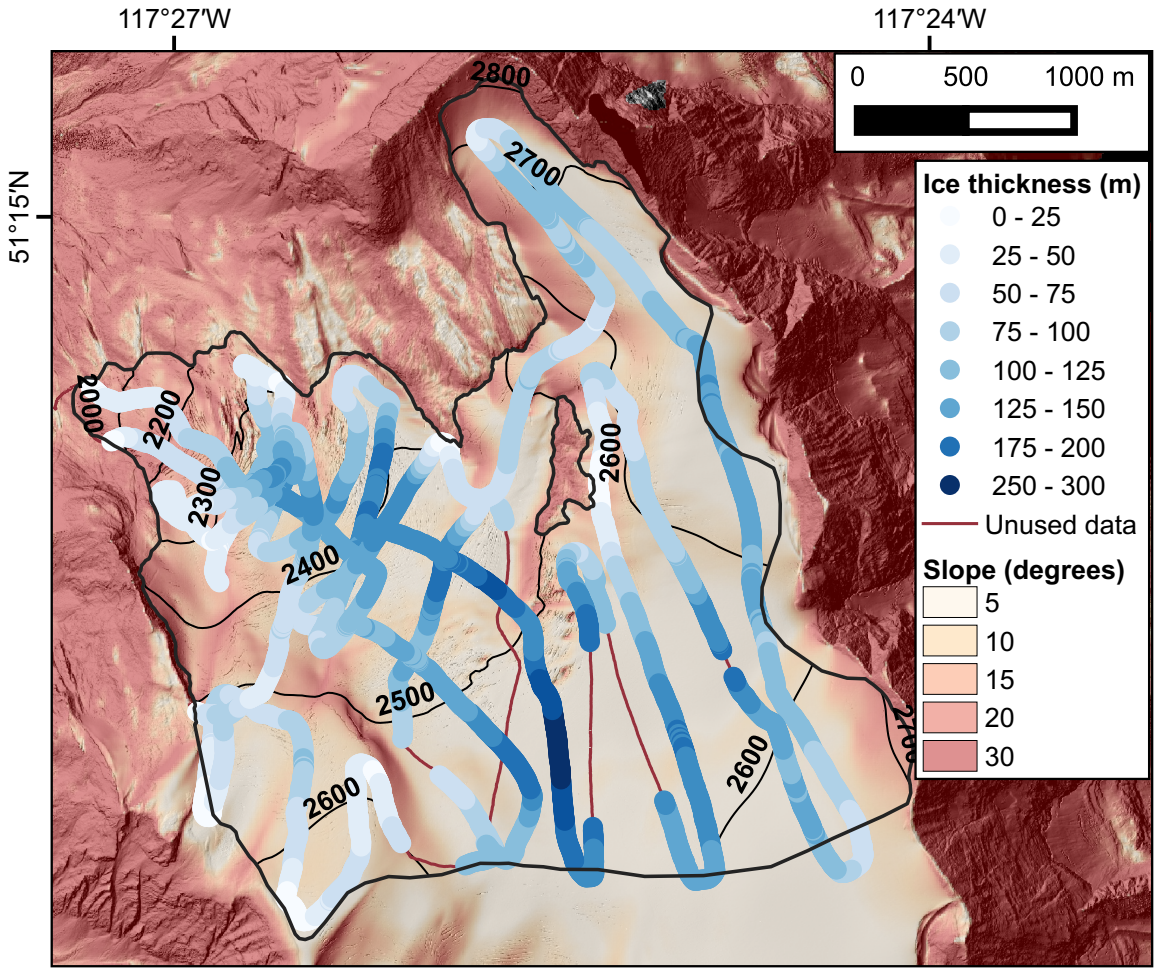

Fig. S1. Ice thickness for Illecillewaet Glacier from radar surveys in 2016 and 2018. Image is a 1-m resolution LiDAR DEM hillshade from September 17, 2017 with slope on a 10-m grid.

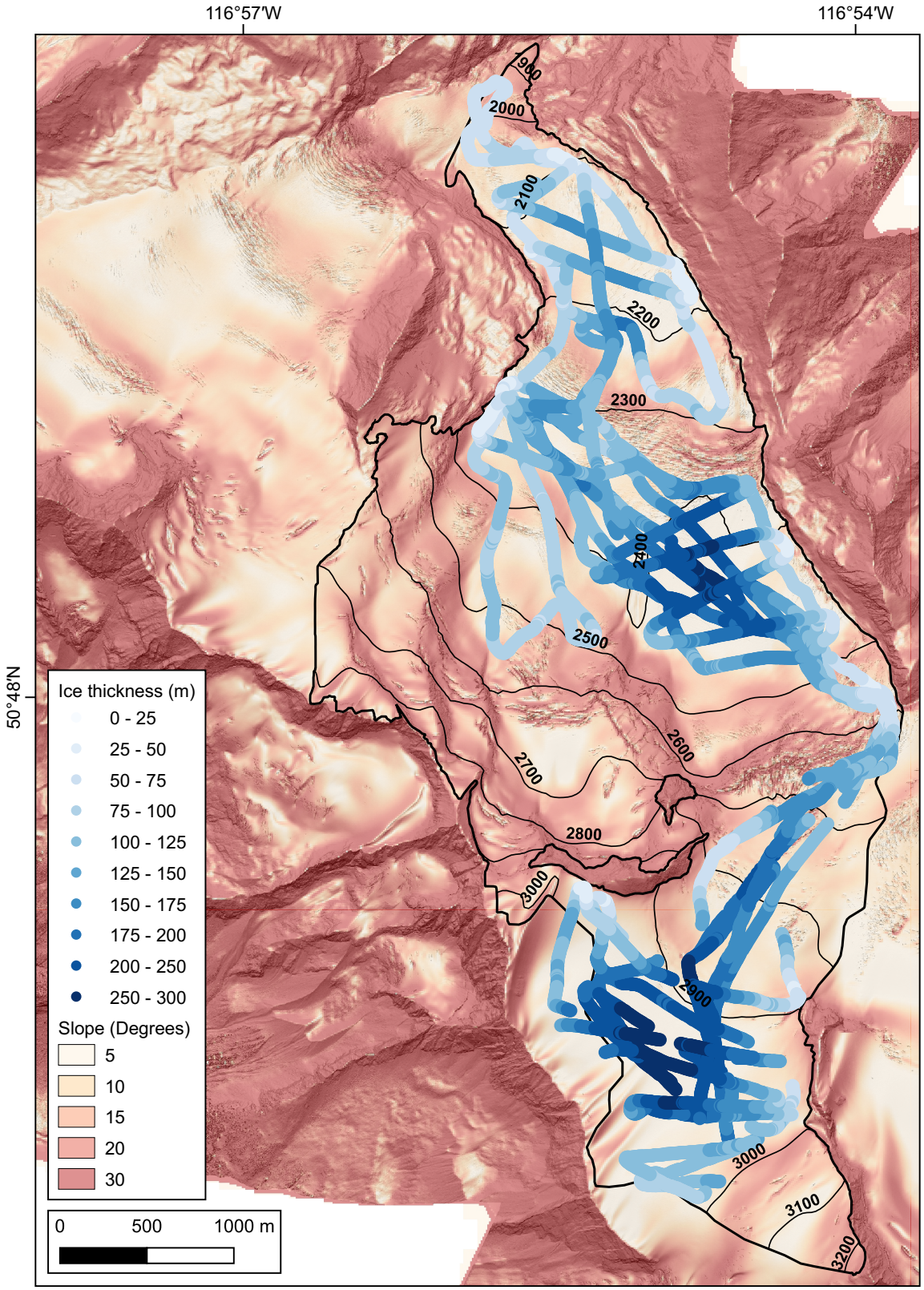

Fig. S2. Ice thickness for Conrad Glacier from radar surveys in 2015, 2016, 2017 and 2018. Image is a 1-m resolution LiDAR DEM hillshade from September 11, 2014 with slope on a 10-m grid.

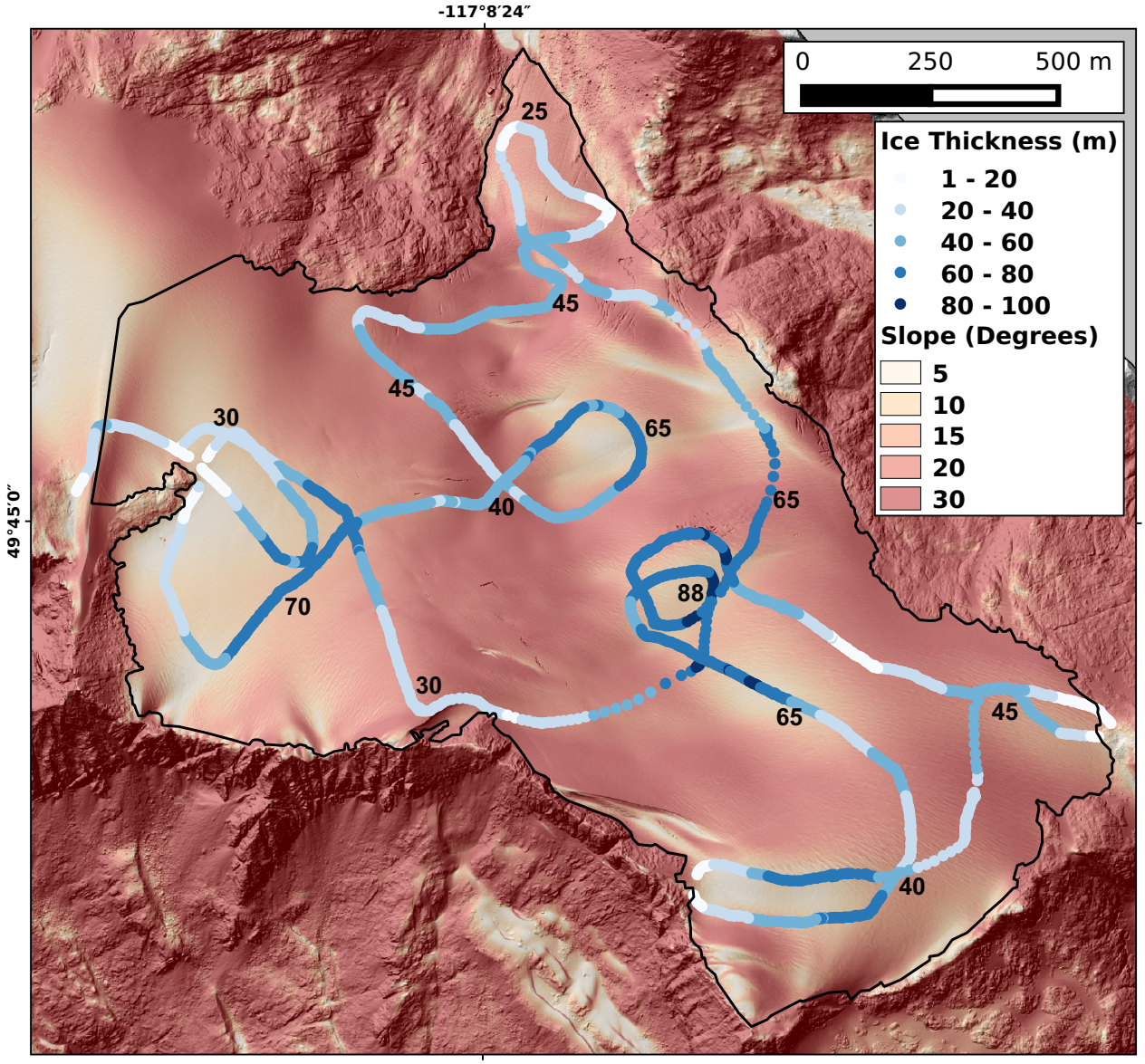

Fig. S3. Ice thickness for Kokanee Glacier from a radar survey in 2017. Image is a 1-m resolution LiDAR DEM hillshade from September 13, 2016 with slope on a 10-m grid.

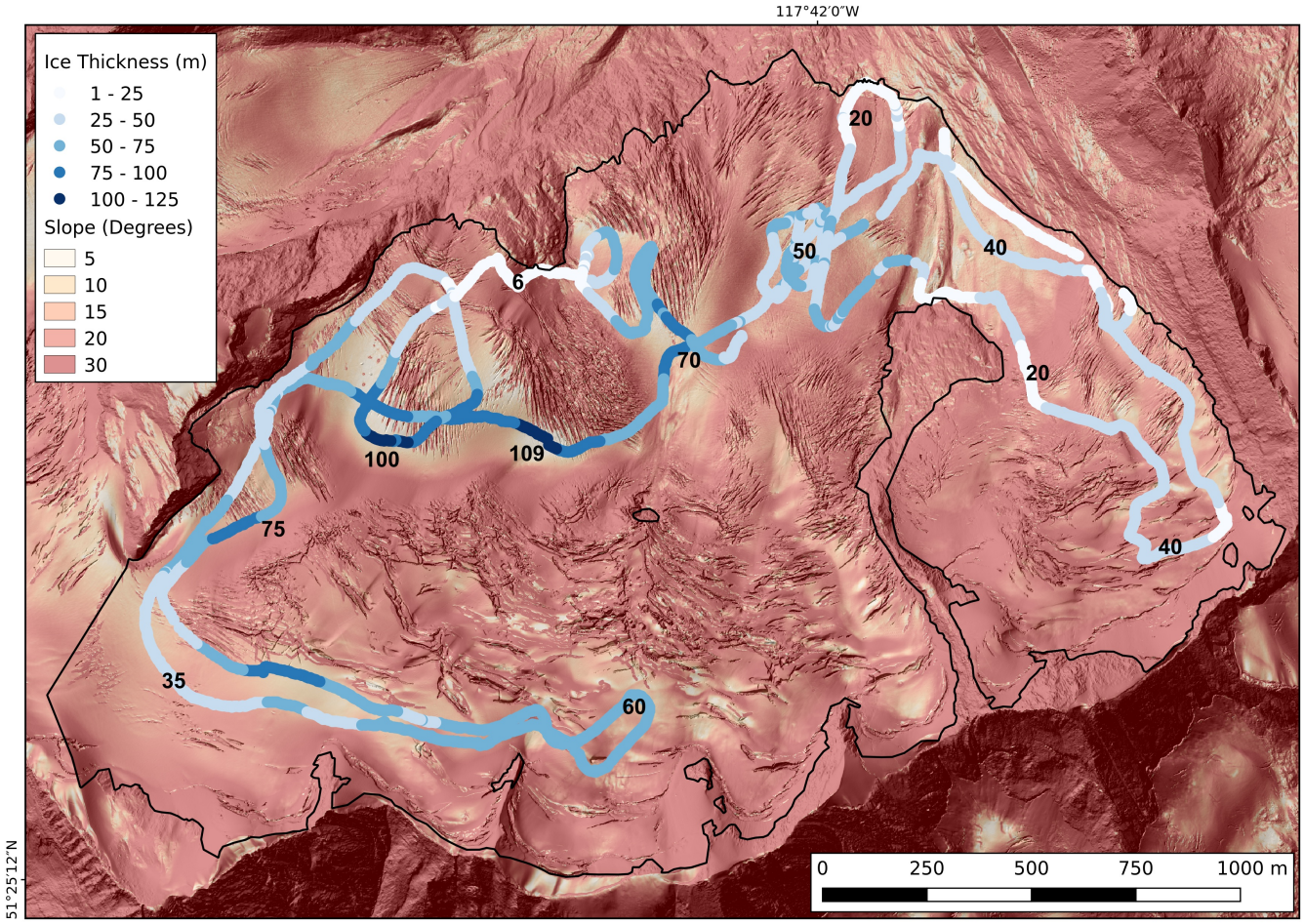

Fig. S4. Ice thickness for Nordic Glacier from a radar survey in 2016. Image is a 1-m resolution LiDAR DEM hillshade from September 11, 2014 with slope on a 10-m grid.

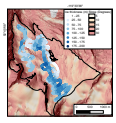

Fig. S5. Ice thickness for Zillmer Glacier from radar surveys in 2016 and 2017. Image is a 1-m resolution LiDAR DEM hillshade from October 3, 2015 with slope on a 10-m grid.

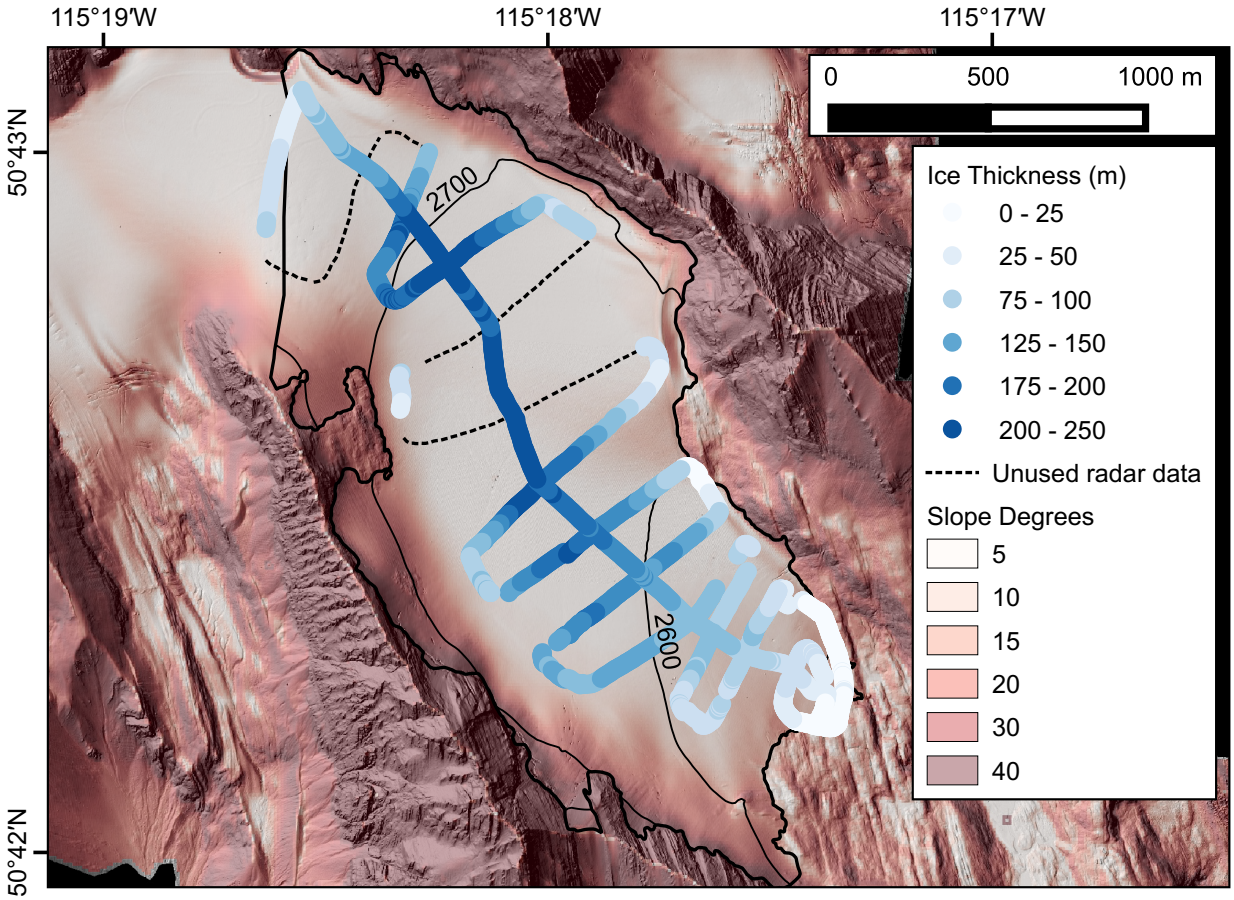

Fig. S6. Ice thickness observations for Haig Glacier from a radar survey in 2009 (Adhikari and Marshall, 2013). Image is a 1-m resolution LiDAR DEM hillshade from September 12, 2015 with slope on a 10-m grid.

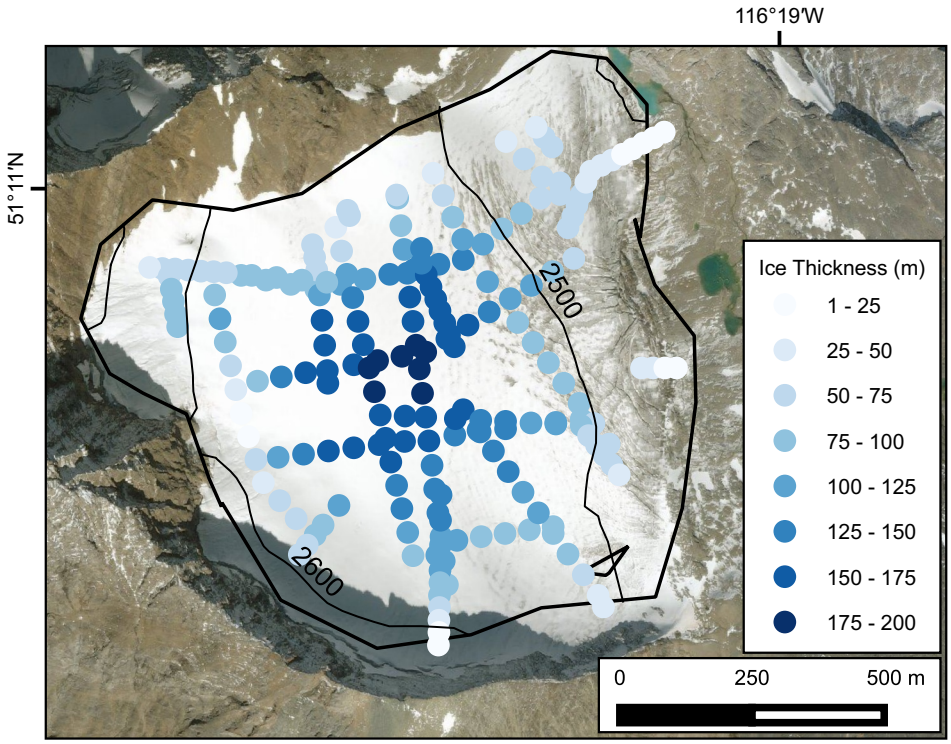

Fig. S7. Ice thickness observations for West Washmawapta Glacier from a radar survey in 2006 (Sanders and others, 2010). Image is from DigitalGlobe from 2008.

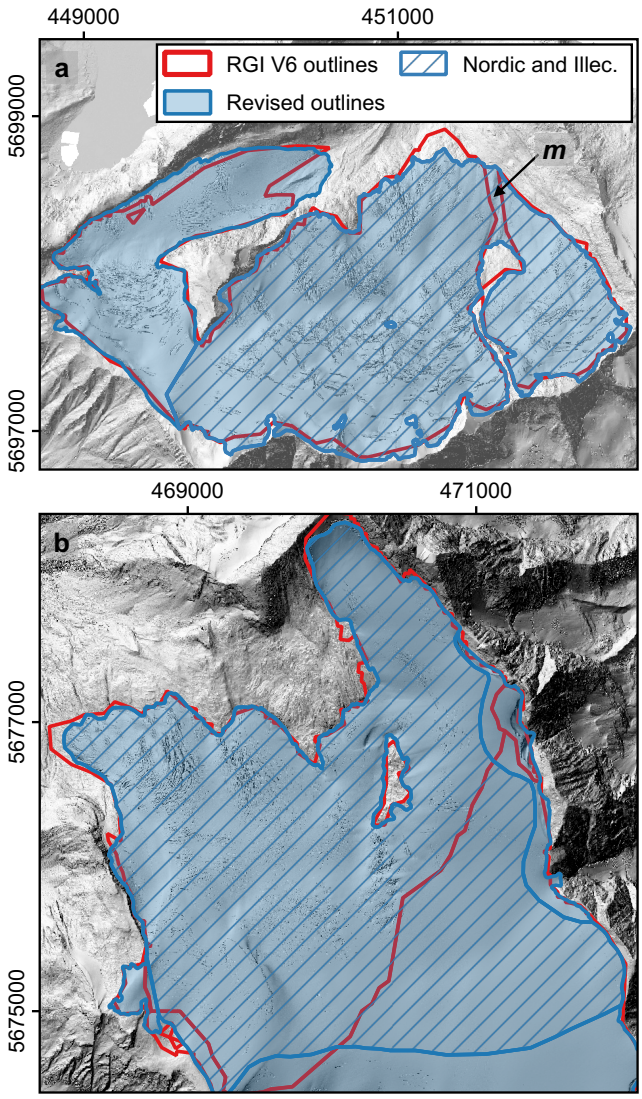

Fig. S8. Outlines of Nordic (a) and Illecillewaet (b) glaciers were both improved to more accurately represent the glaciers' dynamical boundaries. Note the medial moraine (m) is not captured for Nordic Glacier. See Figure S9 for a photo of the medial moraine.

Fig. S9. Photo of the debris-covered medial moraine between the main flowline and eastern branch of Nordic Glacier. This moraine is mapped as bedrock within RGI V6 and thus the eastern branch cannot contribute flux to the terminus.

Separating glacier complexes accurately, such as the Illecillewaet Névé, is a challenge given that many ice divides are in low angle topography. The glacier divides or glacier drainages in British Columbia were separated by Bolch and others (2010) using a 25-m DEM generated by the Terrain Resource Inventory Management (TRIM) program at a scale of 1:20,000. This DEM, built from aerial photographs, often had large artifacts in the accumulation area of glaciers and is responsible for the assignment of a major portion of the accumulation area of Illecillewaet Glacier to neighboring Geikie Glacier (Figure S8).

To improve the polygons of Nordic and Illecillewaet glaciers, used a 1-m LiDAR DEM hillshade and a ΔDEM (Pelto and others, 2019). For Illecillewaet Glacier we ran a watershed algorithm over a 1-m LiDAR DEM to generate the ice divides. Using the watershed algorithm using the SRTM DEM produces a near-identical ice divide to the LiDAR-derived divide. An observed overdeepened trough comprising a major portion of the ice volume of Illecillewaet Glacier is only modeled with the updated polygon (Figure S10).

As defined in RGI V6.0 (2005), Zillmer Glacier has a branch which connects with the glacier at its northwestern edge (Figure S11). In 2015, this connection only spanned 170 m, shrinking to 130 m by 2018. We separated the branches and found little influence on inversion thickness (<2%), consistent with minimal flux. Two new nunataks appeared in 2018: one west of center and one 400 m south of a pre-existing nunatak ridge located east of the center flowline (Figure S11). Given that anomalies between modeled and observed ice thickness exist proximal to these nunataks, we tested updating the glacier outline with the September 30, 2018 LiDAR DEM, which increased the size of the existing nunataks and added the two

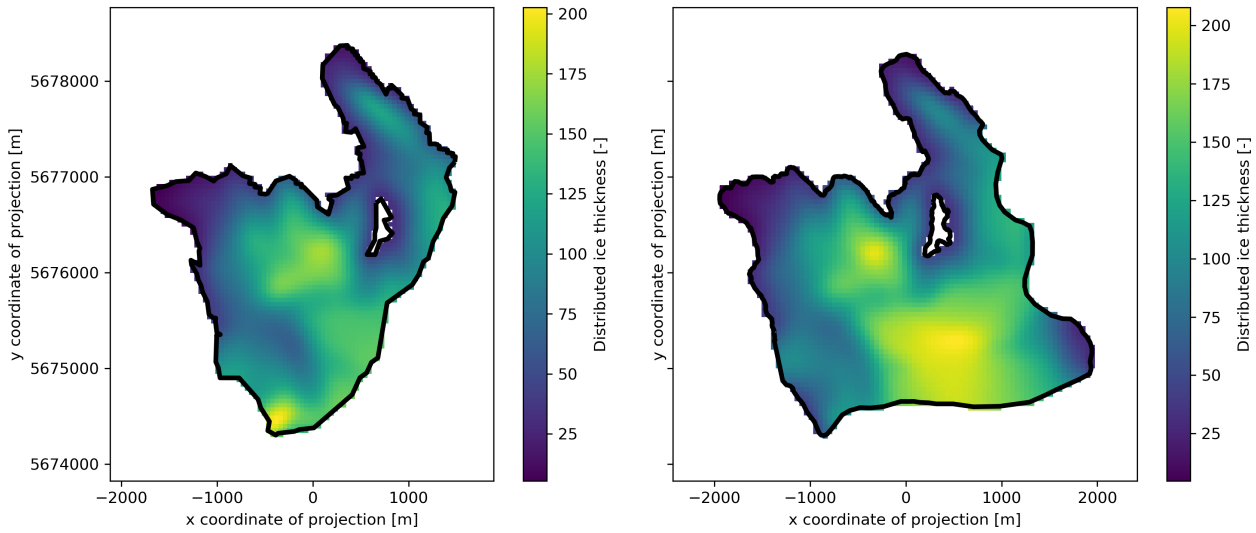

Fig. S10. Illecillewaet Glacier ice thickness with RGI outline (left) versus updated outline (right). Ice thickness increased by 13.2 m (12.2%) with the updated outline.

small nunataks. This had a negligible effect as the new nunataks (200 m^2 and 500 m^2) are too small to alter the modeled ice thickness. Artificially increasing the size of these two nuntaks to 2500 m^2 each, we find that the ice thickness anomalies which exist near the nunataks are only reduced within about a 5-pixel radius of each nunatak, making a small improvement. In OGGM, the distance over which this effect occurs is dictated by the smoothing radius and the distance from a glacier boundary.

With updated outlines we compute new glacier intersects which define ice divides between neighboring glaciers. In OGGM, glacier thickness is interpolated to zero at the outlines without an intersect, thus an intersect is a cue to the model to allow the thickness to be non-zero along the divides.

CROSSOVER ANALYSIS

We compare variable estimates of ice thickness at intersecting radar transects, that is, by crossover analysis, to assess radar measurement uncertainty. For crossover analysis we use 274 intersections with a mean absolute crossover discrepancy in ice thickness of 5.2 $\pm$ 5.8 % (5.2 $\pm$ 5.5 m) (Figure S12)

SMOOTHING PARAMETERS

Accuracy of surface-inversion estimates of ice volume depend on spatial resolution and smoothing of input data (Bahr and others, 2014). To examine the sensitivity of our results to these factors we estimate ice

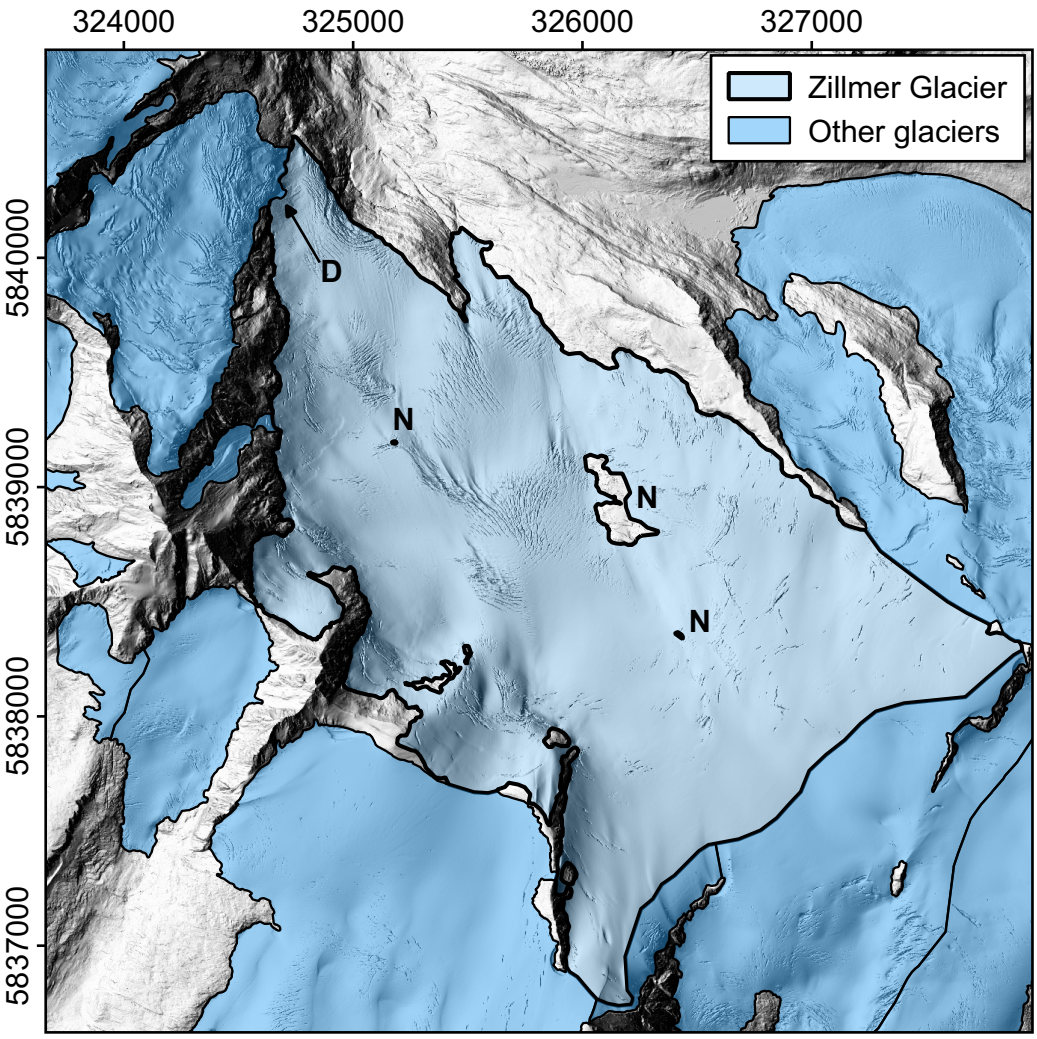

Fig. S11. Zillmer Glacier and area. Nunataks referred to (N) are depicted with the small nunataks appearing first in 2018. We tested dividing the northern arm of Zillmer which connects to the main body of Zillmer (D) and found negligible impact on ice thickness.

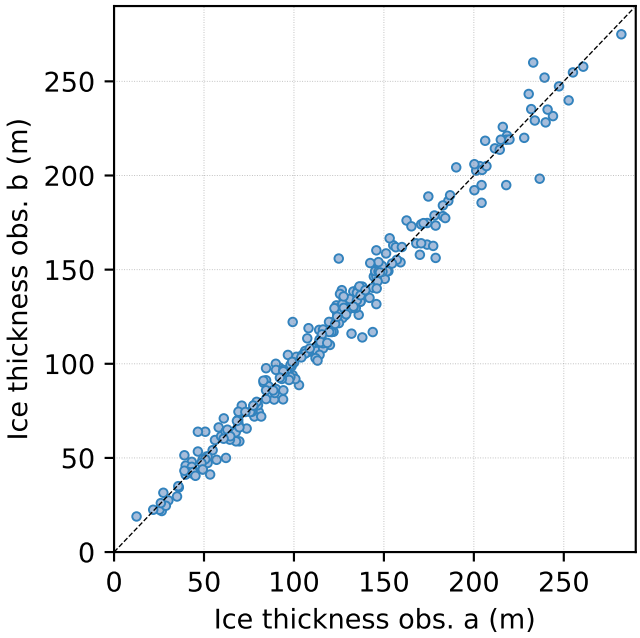

Fig. S12. Estimates of ice thickness at intersecting radar transects (a and b), that is, by crossover analysis. There are 274 intersections or ice thickness pairs, with a mean absolute crossover discrepancy in ice thickness of 5.2 ± 5.8 % (5.2 ± 5.5 m).

volume (1D and 2D) using OGGM with grid resolution between 10–200 m and smoothing parameters influencing the input topography and ice thickness estimates. Smoothing is required for numerical stability (see Bahr and others (2014) for a discussion of the unavoidable trade-off between resolution and accuracy).

We smooth topography by adjusting the smoothing window, which is a Gaussian filter from the grid size of the glacier (23–68 m for our glaciers) up to a resolution of 250 m. Bed elevation estimates are smoothed along the 1D flowlines using a Gaussian filter and we test the default Gaussian kernel (1σ) against no smoothing. The 1D centerline thicknesses are assigned to the 2D glacier according to elevation bands and adding scaling factor which is then normalized. OGGM smooths the final 2D ice thickness estimates by considering the distance from border scaling factor, and the smoothing radius. The scaling factor is based on the distance from the border in meters of each grid cell. The calculated distance from the border is multiplied by a factor proportional to $(\sin\alpha)\frac{n}{n+2}$ at every grid cell; where n=3, the exponent of Glen's flow law (Glen, 1955). The factors are normalized in order to preserve total ice volume. The larger the distance from the border exponent (default: 0.25), the more effect the smoothing parameter has (Figure S13). We vary the distance from the border exponent from 0 to 1.5 by increments of 0.05 (Figure S14). Finally, the smoothing radius determines the window used to smooth the computed ice thickness with a Gaussian filter.

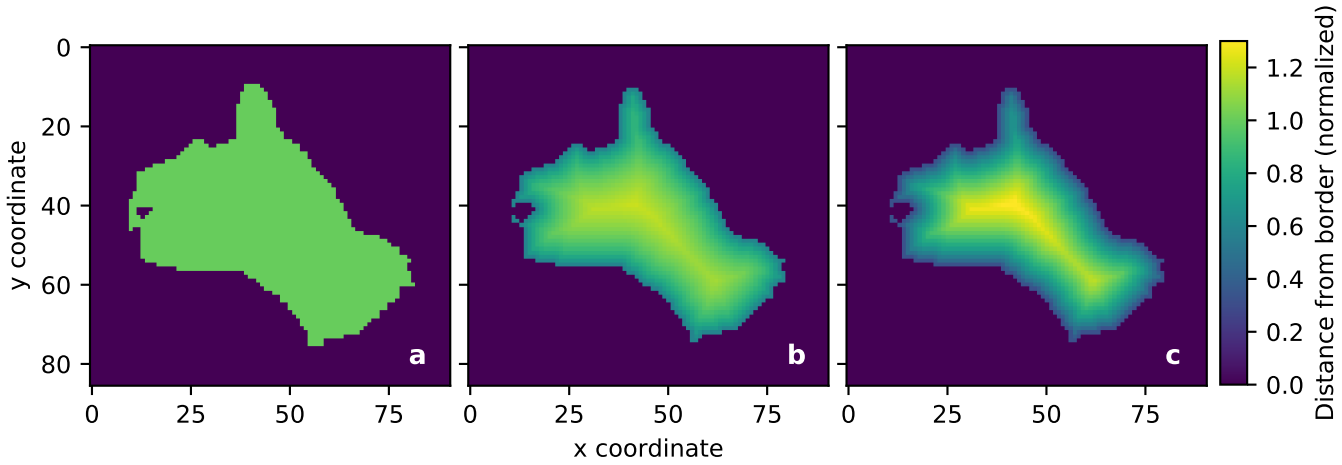

Fig. S13. Normalized distance from border parameter for exponents used to calculate the parameter: 0.00 (a), 0.25 (b), 0.50 (c). Default: 0.25. If 0.00 is chosen, distance from the border is not taken into account. Larger exponents result in a steeper parameter gradient and thus affect the output more.

The smoothing radius default is to use the same window size as the map topography. We test changing the smoothing radius from the grid cell size of each glacier up to 250 m.

The distance from border ice thickness smoothing parameter (Figure S13) reduced MAE. Iterating over the distance from the border exponent and setting A to the optimized value of Table 5, produces minimum MAE with an exponent of 0.17 (Figure S14). The best exponent increases to 0.37 if we use our Basin average A. The distance parameter (Figure S14) essentially has the inverse effect of the of the A parameter, with a larger distance parameter causing ice thickness to taper more from the edges of the glacier inward (Figure S13), just as a small A parameter prescribes stiffer ice, allowing less flow or spreading of the ice. Varying the smoothing window generally showed decreased MAE with increased smoothing window size (Figure S15). Varying the flowline thickness smoothing between no smoothing and the default Gaussian filter kernel (1σ) has marginal effect on estimated ice thickness (< 2 %).

ROCKY MOUNTAIN MASS BALANCE

From 2002–2018, winter balance averaged 1.36 $\pm$ 0.2 m w.e. at Haig Glacier and 1.20 $\pm$ 0.07 m w.e. at Peyto Glacier (Demuth and Keller, 2006) from 1966–1995. From 2014–2018, our study glaciers in the Columbia Mountains received an average of 1.95 $\pm$ 0.08 m w.e. a^{-1} (Pelto and others, 2019), while Haig Glacier received 1.37 m w.e. a^{-1} over the same period. Despite the low accumulation rate, Haig Glacier

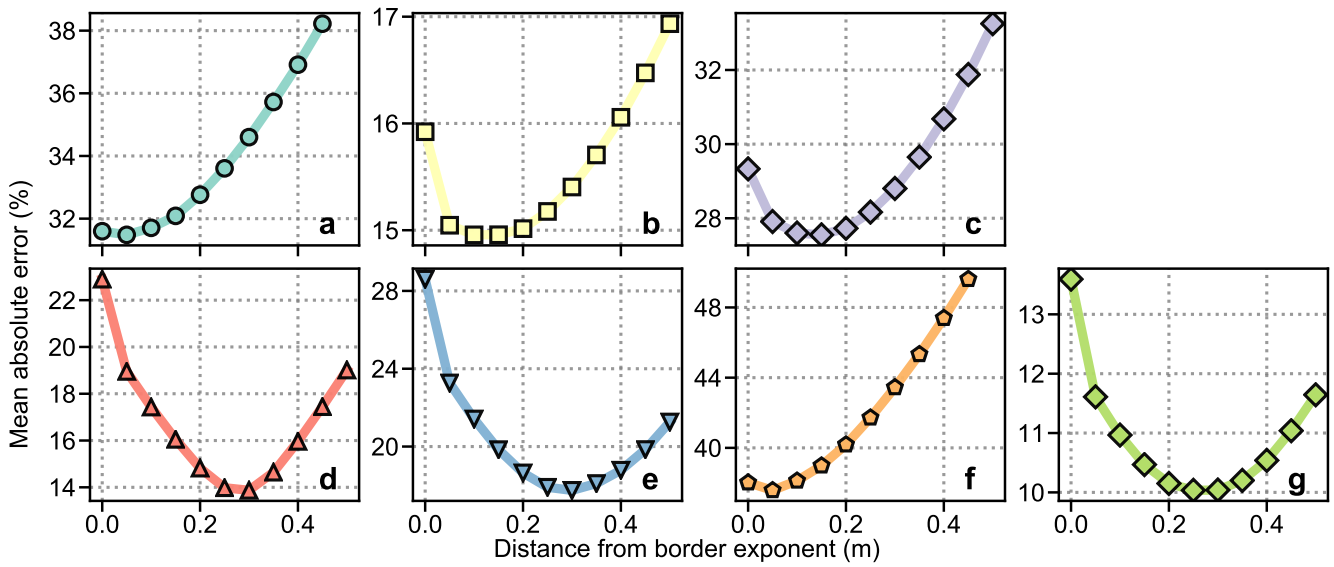

Fig. S14. Distance from border parameter exponents from 0.0 to 0.5 (default: 0.25) against percent error for (a) Zillmer, (b) Nordic, (c) Illecillewaet, (d) West Washmawapta, (e) Haig, (f) Conrad, and (g) Kokanee glaciers. Model run was conducted with the optimized Glen's A parameter and in situ balance gradient for each glacier.

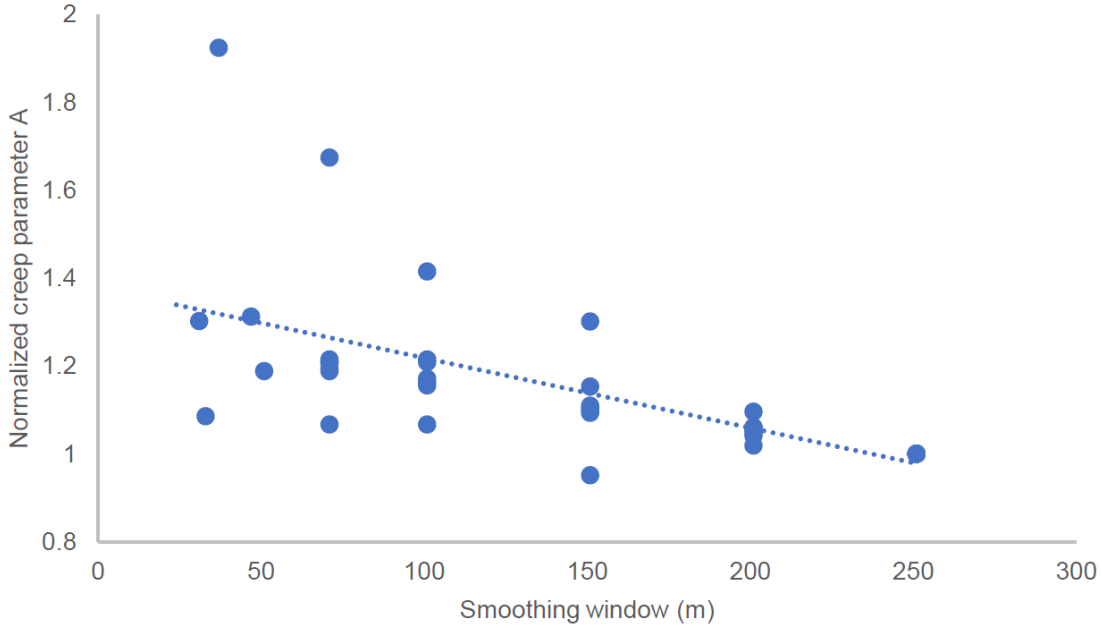

Fig. S15. Smoothing window (m) from the grid cell size of each glacier (23–68 m) to 250 m against optimized A parameter (A_{opt}).

has a steep balance gradient Table 4 perhaps driven by summer balance (Marshall, 2014). Peyto Glacier also has a relatively steep balance gradient, and thus when prescribing the greater in situ balance gradient for West Washmawapta Glacier (to which we assign the average of the balance gradient from Peyto and Haig glaciers). It is likely that the lack of stress gradients is responsible for OGGM deriving lower balance gradients than is observed. However, the equilibrium assumption likely plays a role as well given the relatively lesser snow accumulation of the Rocky Mountains combined with the current disequilibrium of glaciers in the Rocky Mountains (Marshall and others, 2011).

REFERENCES

Adhikari S and Marshall SJ (2013) Influence of high-order mechanics on simulation of glacier response to climate change: Insights from Haig Glacier, Canadian Rocky Mountains. *The Cryosphere*, **7**(5), 1527–1541, ISSN 1994-0424 (doi: 10.5194/tc-7-1527-2013)

Bahr DB, Pfeffer WT and Kaser G (2014) Glacier volume estimation as an ill-posed inversion. *Journal of Glaciology*, **60**(223), 922–934, ISSN 0022-1430 (doi: 10.3189/2014JoG14J062)

Bolch T, Menounos B and Wheate R (2010) Landsat-based inventory of glaciers in western Canada, 1985–2005. *Remote Sensing of Environment*, **114**(1), 127–137, ISSN 00344257 (doi: 10.1016/j.rse.2009.08.015)

Demuth M and Keller R (2006) An assessment of the mass balance of Peyto Glacier (1966–1995) and its relation to recent and past-century climatic variability. *Peyto Glacier: One Century of Science*, **8**, 83–132

Glen JW (1955) The creep of polycrystalline ice. *Proceedings of the Royal Society of London. Series A. Mathematical and Physical Sciences*, **228**(1175), 519–538, ISSN 0080-4630 (doi: 10.1098/rspa.1955.0066)

Marshall SJ (2014) Meltwater run-off from Haig Glacier, Canadian Rocky Mountains, 2002-2013. *Hydrology and Earth System Sciences*, **18**(12), 5181, ISSN 1607-7938

Marshall SJ, White EC, Demuth MN, Bolch T, Wheate R, Menounos B, Beedle MJ and Shea JM (2011) Glacier water resources on the eastern slopes of the Canadian Rocky Mountains. *Canadian Water Resources Journal*, **36**(2), 109–134, ISSN 0701-1784, 1918-1817 (doi: 10.4296/cwrj3602823)

Pelto BM, Menounos B and Marshall SJ (2019) Multi-year evaluation of airborne geodetic surveys to estimate seasonal mass balance, Columbia and Rocky Mountains, Canada. *The Cryosphere*, **13**(6), 1709–1727 (doi: 10.5194/tc-13-1709-2019)

Pfeffer WT, Arendt AA, Bliss A, Bolch T, Cogley JG, Gardner AS, Hagen JO, Hock R, Kaser G, Kienholz C, Miles ES, Moholdt G, Mölg N, Paul F, Radić V, Rastner P, Raup BH, Rich J and Sharp MJ (2014) The Randolph Glacier

Inventory: A globally complete inventory of glaciers. *Journal of Glaciology*, **60**(221), 537–552, ISSN 00221430, 17275652 (doi: 10.3189/2014JoG13J176)

Sanders J, Cuffey K, MacGregor K, Kavanaugh J and Dow C (2010) Dynamics of an alpine cirque glacier. *American Journal of Science*, **310**(8), 753–773, ISSN 0002-9599 (doi: 10.2475/08.2010.03)